



Raman spectroscopy study of the secondary actinolite in gabbrodiorite intrusive rocks from Varan area, Urumieh-Dokhtar Magmatic Arc, Iran

Ghosoun Zheira, Bahman Rahimzadeh*, Fariborz Masoudi

Department of Minerals and Groundwater Resources, Faculty of Earth Sciences, Shahid Beheshti University, Tehran, Iran

Received 6 July 2020; accepted 1 November 2020

Abstract

Mineralogical studies play a key role in deciphering mineral's formation and associated geochemical processes in geosciences. This paper presents the application of Raman spectroscopy to the characterization of actinolite in rock samples. The studied actinolite was formed as the pseudomorph of primary pyroxene in gabbrodiorite intrusive rock sample collected from Varan area, Urumieh-Dokhtar Magmatic Arc of Iran. The Raman spectra of micrometer-sized actinolite grains embedded in a crude rock sample are compared with the corresponding literature data for actinolite and tremolite in range of 200-1200 cm^{-1} and 3600-3700 cm^{-1} region. The results show that the quantitative estimation of $\text{Mg}\# = \text{Mg}/(\text{Mg}+\text{Fe}^{2+})$ can be obtained from the fractional intensities of the OH-stretching bands by applying Raman spectroscopy to micrometer-sized actinolite grains in a crude rough rock sample, which is in good agreement with the results from EMPA. The Raman spectroscopy is a fast method and low-cost for quantitative estimation of $\text{Mg}\#$ in actinolite.

Keywords: Actinolite, Raman spectroscopy, $\text{Mg}\#$, Urumieh-Dokhtar Magmatic Arc, Iran

1. Introduction

The electron microprobe analysis (EMPA) is a standard method to identify minerals subgroups and even mineral species. In recent decades, however, Raman spectroscopy has been considered by many researchers as a fast method to identify most of the rock-forming minerals (Mikouchi and Miyamoto 2000; Wang et al. 2001; Makreski et al. 2005a and b; Šontevska et al. 2008; Makreski et al. 2009; Buzatu and Buzgar 2010; Kaindl et al. 2011; Buzgar et al. 2013; Andò and Garzanti 2014; Apopei et al. 2014; Bersani et al. 2018; Huraiova et al. 2018). Compositional variation for many mineralogical members in the same group like amphibole can also be inferred from Vibrational spectroscopy. The peak positions (the phonon modes) are sensitive to both structure and chemistry (Leissner et al. 2015; Waesermann et al. 2020). Besides, the Raman technique is an analytical method easy to be handled, unexpensive, and can be applied to study minerals in any shapes, e.g., single crystals (Leissner 2014; Susta et al. 2018) as well as in polished sections (Belluso et al. 2007; Majumdar and Mathew 2015; Yazdi et al. 2016). Hence, during the identification of mineral varieties, the Raman spectroscopy is advantageous over the EMPA.

Amphibole members with a double chain of tetrahedral have complex chemical compositions (Hawthorne et al. 2007). However, studies showed that identification of its species is possible by Raman spectroscopy. Raman spectroscopy has been applied to determine amphibole species and characterize their chemical formulae

accurately (Wang et al. 1988 a, b and c; Della Ventura et al. 1991, 1993; Bard et al. 1997; Kloprogge et al. 2001a and b; Chen et al. 2004; Gopal et al. 2004; Rinaudo et al. 2004; Makreski et al. 2006; Petry et al. 2006; Rinaudo et al. 2006; Fornero et al. 2008; Apopei and Buzgar 2010; Apopei et al. 2011; Leissner 2014; Sbroscia et al. 2018; Waesermann et al. 2020; Ivanov et al. 2019).

Different researchers attribute the observed peaks in amphibole to different modes (Andrut et al. 2000; Shurvell et al. 2001; Makreski et al. 2006; Jovanovski et al. 2009; Yazdi et al. 2019). However, Apopei and Buzgar (2010) briefly presented a review of the vibrational modes in amphibole.

In addition, a detailed Raman-scattering study on the OH-Stretching range has been applied by Leissner et al. (2015) for several samples of different amphibole subgroups. It is shown that the spectra of OH-stretching vibration could be a useful tool for exact mineral identification. The OH group shares O with a triplet of $\text{M}_1\text{M}_1\text{M}_3$ octahedral in the C site. Therefore, the OH stretching range peaks are related to the various chemical configurations of the adjacent $\text{M}_1\text{M}_1\text{M}_3$ octahedra. The number of peaks and their intensities are used to gain information about the arrangement of cations on C site (Ernst and Wai 1970; Kloprogge et al. 2001a). Based on infrared spectroscopic of clinoamphibole, Burns and Strens (1966) studied the effect of substitution of Fe^{2+} for Mg^{2+} in M_1 and M_3 sites on the position of the OH bond-stretching mode, which causes the appearance of peaks at lower frequencies as compared to the OH stretching peak of pure ${}^{\text{C}}\text{Mg}^{2+}$ (MgMgMg). Leissner et al. (2015) reported a good agreement between infrared and Raman peak positions related to the same chemical species.

*Corresponding author.

E-mail address (es): b_rahimzadeh@sbu.ac.ir

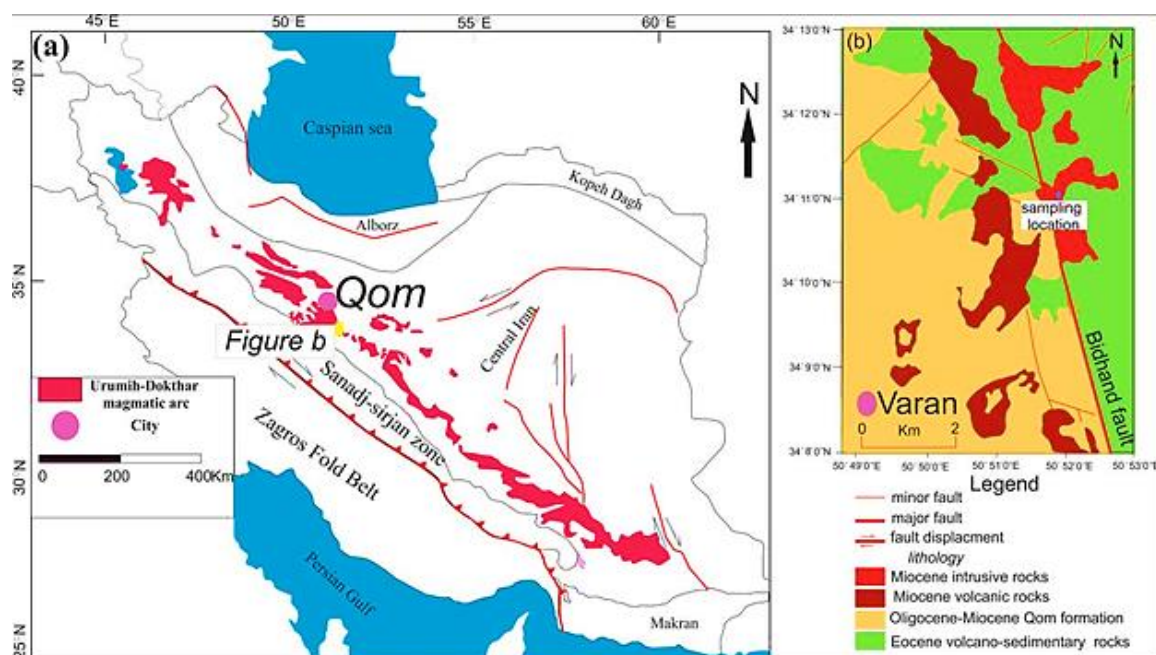


Fig 1. (a) Simplified geological map of Iran, showing major tectonic units (modified after Alavi 1994), (b) Simplified geological map of Varan area (modified after Ghalamghash and Babakhani 1996).

However, in all previous studies, the comparison of results and compositional identification and structural characteristics of different minerals from the amphibole group inferred from a Raman spectral record obtained with a precisely calibrated high-resolution spectrometer and special sample preparation and orientation (e.g., see Waesermann et al. 2020). Generally, the intensity of the Raman bands depends on the sample's orientation for the laser incident beam (Fornero et al. 2008; Leissner 2014; Waesermann et al. 2020). Few studies focused on the Raman spectral characteristics of tremolite-actinolite-ferro-actinolite series (Makreski et al. 2006; Apopei and Buzgar 2010; Apopei et al. 2011; Bersani et al. 2019). Actinolite is a solid solution composition between the end-member of the tremolite and ferro-actinolite series. According to Leake et al. (2003 and 2004), the solid solutions with the ratios of $Mg/(Mg + Fe^{2+}) \geq 0.90$ are tremolite, between 0.50 and 0.90 actinolite, and less than 0.50 ferro-actinolite. In the present study, actinolites from Varan area in the central part of Urumieh-Dokhtar Magmatic Arc (UDMA) of Iran are examined by Raman spectroscopy on a non-prepared rough sample and in random crystallographic orientations. We assume that the compositional characteristics of secondary actinolite can be obtained from a Raman spectral recorded without special sample preparation of a rough crystallized geological sample.

2. Geology and petrography study

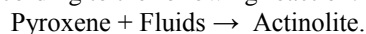
Actinolite occurs as a secondary mineral in the gabbrodiorite intrusive rocks from Varan area in the central part of Urumieh-Dokhtar Magmatic Arc (UDMA) of Iran (Fig 1a). Varan area is located at 60 Km to South of Qom city. Three major geological units characterized this area from

oldest to newest in time: 1) Eocene volcano-sedimentary rocks; 2) Qom Formation that composed of marine limestone and marl sediments; 3) the Miocene volcanic and intrusive rocks (Fig 1b). The intrusions rang in composition from intermediate to acidic rocks, dominated by gabbrodioritic rocks that consist of millimeter-sized plagioclase, amphibole and pyroxene as main minerals. Amphiboles are present as both primary and secondary types. The primary amphiboles (Hornblende) are euhedral to subhedral in shape with brownish-yellow colors. The secondary amphibole is actinolite, which may be formed as a pseudomorph of pyroxene (Fig 2).



Fig 2. Photomicrographs of the gabbrodioritic rock in Varan area show the primary amphiboles (Hornblende) and secondary actinolite, which is a pseudomorph of primary pyroxene. Mineral abbreviations based on Whitney and Evans (2010): Hbl: Hornblende; Act: Actinolite; Pl: plagioclase; Opq: opaque.

Castro and Stephens (1992) conclude that the actinolite in calc-alkaline granitic rocks and their micro-granular enclaves is, in fact, a pseudomorph after primary pyroxene. Pyroxene reacted in the solid-state to form actinolite, presumably in the presence of a fluid phase according to the following reaction:



3. Methods

3.1. Electron Microprobe

Quantitative electron microprobe analysis of actinolite was determined by a JEOL JXA8230 5-WDS electron microprobe at the department of earth sciences, University of Toronto, Canada. During operation, accelerating voltage, beam current and beam diameter were 20 kV, 20 nA, and 3 μm , respectively. Three points from each sample have been analyzed (Table 1a).

Table 1a. Chemical composition (wt.%) of actinolite crystals in the gabbrodioritic rocks, determined by electron microprobe analysis

	K17_cc1_1	K17_cc1_2	K-17-cc1-3	K17_cc2_1	K17_cc2_2	K17_cc2_3
SiO ₂	51.40	51.38	52.91	53.81	53.01	53.09
TiO ₂	0.64	0.61	0.51	0.23	0.40	0.56
Al ₂ O ₃	2.69	2.65	2.53	1.16	1.78	2.52
FeO (t)	10.19	10.52	10.53	9.61	9.60	9.44
MgO	17.92	17.73	18.13	19.38	18.32	19.05
MnO	0.57	0.68	0.71	0.61	0.39	0.40
CaO	11.45	11.25	10.82	10.81	11.81	11.17
Na ₂ O	0.77	0.67	0.62	0.25	0.48	0.50
K ₂ O	0.18	0.16	0.12	0.07	0.19	0.14
OH	4.19	4.34	3.12	4.07	4.03	3.13
Σ (wt%)	100.00	100.00	100.00	100.00	100.00	100.00

Table 1b. The crystal-chemical formulae of actinolite with calculations $X_{\text{EMPA}} = {}^{\text{c}}(\text{Mg}/(\text{Mg}+\text{Fe}^{2+}))$.

sample	Name (IMA2012)	Chemistry:	AB2C5T8O22W2	$X_{\text{EMPA}} =$ ${}^{\text{c}}(\text{Mg}/(\text{Mg}+\text{Fe}^{2+}))$
K17_cc1_1	actinolite	$(\square\text{Na}_{0.109}\text{K}_{0.032})\Sigma 0.141$	$(\text{Ca}_{1.772}\text{Na}_{0.107}\text{Mn}_{0.07}\text{Fe}^{2+}_{0.051})\Sigma 2$	0.85
K17_cc1_2	actinolite	$(\text{Mg}_{3.862}\text{Fe}^{2+}_{0.671}\text{Fe}^{3+}_{0.467})\Sigma 5$	$(\text{Si}_{7.429}\text{Al}_{0.458}\text{Ti}_{0.07}\text{Fe}^{3+}_{0.043})\Sigma 8$ O ₂₂ ((OH) ₂) $\Sigma 2$	0.83
K17_cc1_3	actinolite	$(\square\text{Na}_{0.067}\text{K}_{0.034})\Sigma 0.101$	$(\text{Ca}_{1.822}\text{Na}_{0.066}\text{Fe}^{2+}_{0.064}\text{Mn}_{0.047})\Sigma 1.999$	0.83
K17_cc2_1	actinolite	$(\text{Mg}_{3.932}\text{Fe}^{2+}_{0.778}\text{Fe}^{3+}_{0.291})\Sigma 5$	$(\text{Si}_{7.631}\text{Al}_{0.303}\text{Ti}_{0.043}\text{Fe}^{3+}_{0.023})\Sigma 8$ O ₂₂ ((OH) ₂) $\Sigma 2$	0.87
K17_cc2_2	actinolite	$(\square\text{Na}_{0.087}\text{K}_{0.022})\Sigma 0.109$	$(\text{Ca}_{1.658}\text{Fe}_{0.17}\text{Mn}_{0.086}\text{Na}_{0.086})\Sigma 2$	0.84
K17_cc2_3	actinolite	$(\text{Mg}_{3.864}\text{Fe}^{2+}_{0.78}\text{Fe}^{3+}_{0.309}\text{Ti}_{0.047})\Sigma 5$	$(\text{Si}_{7.566}\text{Al}_{0.426}\text{Ti}_{0.008})\Sigma 8$ O ₂₂ ((OH) ₂) $\Sigma 2$	0.87
		$(\square\text{Na}_{0.035}\text{K}_{0.012})\Sigma 0.047$	$(\text{Ca}_{1.66}\text{Fe}^{2+}_{0.23}\text{Mn}_{0.075}\text{Na}_{0.035})\Sigma 2$	0.87
		$(\text{Si}_{7.714}\text{Al}_{0.196}\text{Fe}^{3+}_{0.065}\text{Ti}_{0.025})\Sigma 8$	O ₂₂ ((OH) ₂) $\Sigma 2$	0.84
		$(\square\text{Na}_{0.095}\text{K}_{0.03})\Sigma 0.125$	$(\text{Ca}_{1.748}\text{Na}_{0.094}\text{Mn}_{0.083}\text{Fe}^{2+}_{0.075})\Sigma 2$	0.87
		$(\text{Mg}_{3.832}\text{Fe}^{2+}_{0.714}\text{Fe}^{3+}_{0.454})\Sigma 5$	$(\text{Si}_{7.448}\text{Al}_{0.453}\text{Ti}_{0.067}\text{Fe}^{3+}_{0.032})\Sigma 8$	0.87
		$(\square\text{Na}_{0.069}\text{K}_{0.025})\Sigma 0.094$	$(\text{Ca}_{1.701}\text{Fe}^{2+}_{0.182}\text{Na}_{0.069}\text{Mn}_{0.049})\Sigma 2.001$	0.87
		$(\text{Mg}_{4.036}\text{Fe}^{2+}_{0.592}\text{Fe}^{3+}_{0.348}\text{Ti}_{0.024})\Sigma 5$	$(\text{Si}_{7.543}\text{Al}_{0.422}\text{Ti}_{0.035})\Sigma 8$ O ₂₂ ((OH) ₂) $\Sigma 2$	

* \square : vacant A site

3.2. Raman spectroscopy

In the present study, Raman spectroscopy was applied to micrometer-sized actinolite grains in a crude rough rock sample (K-17). Two actinolite grains were investigated by the Raman spectroscopy, and two representative spectra were presented.

The actinolite Raman spectra were recorded using a Takram P50C0R10 Raman Microscope equipped with a Hamamatsu detector at the gemology Laboratory at the Shahid Beheshti University of Tehran, Iran. An Nd: YAG laser ($\lambda = 532$ nm, Laser Power = 100 mW) was used to excite the Raman scattering. The system was calibrated using the 520.5 cm^{-1} Raman band of silicon. The spectral resolution was ~ 6 cm^{-1} and spatial Resolution (μm) was ~ 1 . The laser radiation was focused on a diameter of 14 μm by a 60 \times upright microscope objective on the selected crystals. The Raman spectra acquisition time was 1 min. For the range of 200–1200 cm^{-1} and OH stretching range of 3600–3800 cm^{-1} , background correction and peak fitting operations have been performed by Lorentz and Voigt functions, respectively, using the origin software.

4. Result

4.1. Chemical composition

The amphibole name was determined according to the new amphibole nomenclature IMA 2012 (International Mineralogical Association, Hawthorne et al. 2012), using the excel spreadsheet of Locock (2014) as presented in Table 1b.

The EMPA results of actinolite indicate that Mg occurs as dominated octahedral cation with the concentration of 3.66–4.36 apfu. Total Fe content in examined actinolites varies from 1.12 to 1.26 apfu. Values for Ca are higher than > 1 (1.66–1.82 apfu), while Al < 0.5 . Ti, Mn, Na contents are insignificant (Table 1b). Low Al and Ti content can reflect the low pressure and temperature of formation of amphibole receptively (Otten 1984; Anderson and smith 1995). The Mg# (X) = ${}^{\text{c}}\text{Mg}/{}^{\text{c}}(\text{Mg}+\text{Fe}^{2+})$ calculated based on EMPA data, varies between 0.83 to 0.87.

4.2. Results of Raman Spectroscopy

Figure 3 shows the representative Raman spectra of actinolite in studied gabbrodiorite, compared with an actinolite reference Raman spectra (R050336) from RRUFF project (<https://rruff.info>), which has a chemical composition similar to our actinolites in the 200-1200 cm^{-1} region. The Raman bands presented for studied samples are identified on the basis of the description proposed in Apopei and Buzgar (2010). The vibrational assignments of the peaks are given in Table 2.

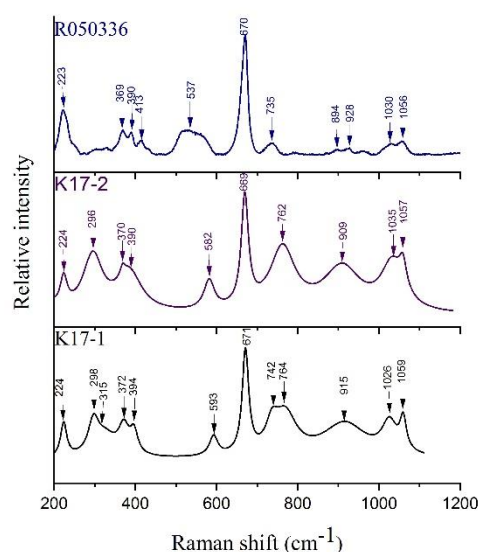


Fig 3. Raman spectra of studied actinolite samples (K17-1 and K17-2) in the 200-1200 cm^{-1} region compared with actinolite reference (R050336) spectra from RRUFF project.

In the region of internal vibrations (625-1200 cm^{-1}), a very intense sharp band appears at 671 cm^{-1} for K17-1 and 669 cm^{-1} for K17-2, due to the symmetric stretching vibration (ν_s) of the Si-O_b-Si bridge. The bands (671 and 669 cm^{-1}) registered in our spectrum is similar to the literature data (Table 2) for actinolite mineral

For the K17-1 sample, one peak of medium intensity split into the component at 742 and 764 cm^{-1} , while the Raman spectrum of the sample of K17-2 actinolite shows only one peak at 762 cm^{-1} . According to Apopei and Buzgar (2010), this band is debatable, given the fact that 750 cm^{-1} is the limit of stretching vibrations (ν_s) of the Si-O_b-Si and O-Si-O modes.

Within symmetric stretching of O-Si-O linkage, the main and broad bands at 915 (K17-1) and 905 cm^{-1} (K17-2) deviated by ~ 12 to 20 cm^{-1} , respectively, compared to the calculated peak at 928 cm^{-1} for RRUFF database (R050336, Fig 3).

The asymmetric stretching vibrations (ν_{as}) of the Si-O_b-Si bridges (1000-1200) exhibit two bands with medium intensity at 1026 and 1059 cm^{-1} for K17-1 and 1035 and 1057 cm^{-1} K17-2, which are also in good agreement with the literature data for actinolite and tremolite species (Table 2).

Lower frequencies below 625 cm^{-1} several bands of medium to weak intensity are observed (Fig 3). The peaks due to the lattice modes appear in the lowest frequency region below 300 cm^{-1} . The most prominent bands due to the lattice modes are observed at 224 and 298 or 296 cm^{-1} with medium intensity. In addition, the peak 298 cm^{-1} has a clearly visible shoulder at ~315 cm^{-1} . The bands situated at 372, 394 cm^{-1} for the K17-1 sample and 370, 390 cm^{-1} for K17-2 sample are assigned to M-OH vibration.

Table 2. Wavenumbers and assignment bands observed in the Raman spectra of a studied sample in the 200-1200 cm^{-1} spectral region, in addition to compare the results with literature data for actinolite and tremolite.

Band assignment	This study		Actinolite				Tremolite	
	K17-1	K17-2	Shurvell*	Huang	Apopei & Buzgar	Apopei et al.	Makreski et al.	Apopei & Buzgar
Lattice mode	224, 298	224, 296	-	222, 231, 249, 263, 303	222, 292	226, 247, 294	222, 248, 303	225, 252, 290
M-O where M= Ca, Mg, Fe2+	372, 394	370, 390	350, 369, 392, 415, 436	348, 371, 393, 415, 434	369, 392, 415	369, 392, 415	346, 368, 391, 413, 433	351, 372, 394, 415, 438
Deformation mode of Si ₄ O ₁₁	-	-	513, 532	529	484, 522	482, 522,	477, 517, 527	483, 528
OH libration/translation	593	582	-	-	581	577	-	-
ν_s (Si-O _b -Si)	671	669	673	673	670	670	672	675
ν_s (Si-O _b -Si)	742, 764	762	740, 749	749	744	744	744	746
ν_s (O-Si-O)	915	909	930, 947	929, 947	928, 946	929, 949	899, 926, 954	928, 949
ν_s (O-Si-O)?	-	-	-	-	-	-	-	-
ν_{as} (Si-O _b -Si)	1026, 1059	1035, 1057	1029, 1058	1027, 1057	1027, 1059	1027, 1059	1026, 1056	1028, 1060
VS-CO ₃	-	-	-	-	-	-	-	1087

Abbreviation: ν_s : symmetric stretching, ν_{as} : asymmetric stretching, O_b: bridging O. * Shurvell et al. (2001), Huang (2003), Apopei and Buzgar (2010: S.no 2-3 for Actinolite and S.no 2-8 for Tremolite), Apopei et al. (2011), Makreski et al. (2006).

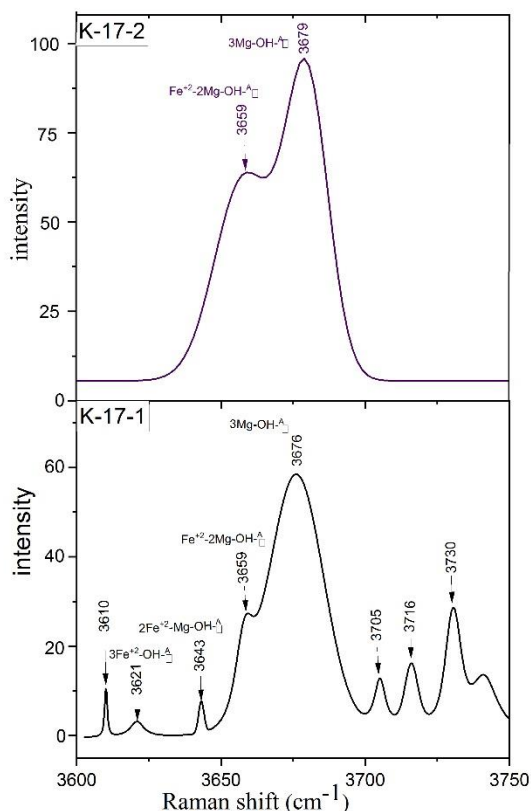


Fig 4. Raman scattering of studies samples caused by OH-stretching modes.

It is noted that the band $\sim 416\text{ cm}^{-1}$ is absent in both Raman spectra of our samples, which is probably due to the orientation of the crystallographic axis with respect to the polarization of the incident light. The 450-625 cm^{-1} region is characterized by the appearance of one main peak at 593 cm^{-1} for K17-1 and 582 cm^{-1} for K17-2. According to Apopei and Buzgar (2010), these bands are characteristic for the vibration of the OH⁻ liberation/translation mode, but recently, Ivanov et al. (2019) have assigned several Raman peaks in the 450-625 cm^{-1} region to a superposition of $M^{(2)}\text{Fe}^{3+}\text{-O}$ bond stretching and Si-O-Si bending vibrations.

The OH bond-stretching mode slightly differ in the amphibole species when different cations are coordinated to the hydroxyl group. Therefore, the Mg, Fe²⁺ composition of the M₁M₁M₃ triplet would have a huge effect on the OH bond-stretching mode and reflect more than one vibration with different intensity (e.g., MgMgMg-OH-A, MgMgFe²⁺-OH-A, MgFe²⁺Fe²⁺-OH-A, and Fe²⁺Fe²⁺Fe²⁺-OH-A) in the OH stretching region. The Raman peaks of studied samples in the 3600-3800 cm^{-1} spectral region are presented in Figure 4 and Table 3.

In K17-1 spectrum, a high intensity band is found at 3676 cm^{-1} . This strong band has been attributed to the MgMgMg-OH-A vibration (where Mg is present in all octahedral M₁M₁M₃ sites). The band at $\sim 3659\text{ cm}^{-1}$ is ascribed to the Fe²⁺MgMg-OH-A in literature data (where either M₃ or one of the M₁ sites is occupied by Fe²⁺). The weak band at 3643 cm^{-1} can be related to the MgFe²⁺Fe²⁺-OH-A vibration, whereas the broader and very weak band at 3621 cm^{-1} related to the Fe²⁺Fe²⁺Fe²⁺-OH-A configuration. In the second sample of actinolite (K17-2) only two bands appear at 3679 and 3659 cm^{-1} , which are assigned to the MgMgMg-OH-A and Fe²⁺MgMg-OH-A vibrations, respectively.

The additional very weak band at 3610 cm^{-1} is attributed to the cations combination involving the replacement of Fe²⁺ with Fe³⁺ in M site, being in accordance with the literature data for actinolite mineral (Burns and Greaves 1971). Moreover, according to many researchers (Yang et al. 1999; Makreski et al. 2006; Iezzi et al. 2007; Su et al. 2009; Leissner et al. 2015; Sbroscia et al. 2018), the appearance of weak bands in the higher region of the OH-stretching vibration, between 3690 to 3730 cm^{-1} , indicates the presence of a partial occupation of A-site (by Na and/or K). Therefore, the bands at 3705, 3716, and 3730 cm^{-1} are related to the stretching of the groups present adjacent to a filled A site, i.e., these bands are assigned to M₁M₁M₃-OH-A configuration. These bands do not appear in the Processed Raman spectrum of K17-2 sample. The 3700-3800 cm^{-1} region of the K17-2 raw spectra presents a very low signal-to-noise ratio.

Table 3. The position of the M₁M₁M₃-OH Raman bands (in cm^{-1}) and compared them with literature data (which observed in Raman and infrared spectra by others).

	Fe ²⁺ Fe ²⁺ Fe ²⁺ -OH-A	Fe ²⁺ Fe ²⁺ Mg-OH-A	Fe ²⁺ MgMg-OH-A	MgMgMg-OH-A
This study: K17-1	3621	3643	3659	3676
This study: K17-2	-	-	3659	3679
Apopei et al. 2011 (actinolite)	-	3647	3660	3674
Apopei et al. 2011 (actinolite)	-	-	3660	3675
Makreski et al. 2006 (tremolite)	-	-	3659	3673
Shurvell et al. 2001 (actinolite)	-	3644	3659	3673
Wilkins 1970 (actinolite)	3625	3643	3660	3665

5. Discussion

In general, all the bands between 200 and 1200 cm^{-1} in the present study (despite some bands shifted or some bands absent and/or some bands show less difference in the intensity due to our operational conditions) are found in the literature for both actinolite and tremolite minerals (Table 2). Generally, the band in the 650-750 cm^{-1} domain is very characteristic for many amphibole minerals (Wang et al. 1988a; Della Ventura et al. 1991 and 1993; Makreski et al. 2006). The most striking difference between the Raman spectra of tremolite and actinolite in the 200-1200 cm^{-1} region lies in the shifting of the strong sharp band to a higher frequency in tremolite, namely, from 670 cm^{-1} in actinolite to 675 cm^{-1} in tremolite (Apopei et al. 2011). Since the strong sharp band due to the ν_3 Si-O_b-Si vibration appears at $\sim 670 \text{ cm}^{-1}$ it could imply that the studied crystals are rather an actinolite than tremolite.

In many studies (e.g., Burns and Greaves, 1971; Gopal et al. 2004; Makreski et al. 2006; Apopei et al. 2011), the importance of 3600-3700 cm^{-1} spectral region has been proven in the distinction between tremolite and actinolite minerals. The main difference between tremolite and actinolite is the $^{\text{C}}\text{Fe}^{2+}$ and $^{\text{C}}\text{Mg}$ content. Depending on the presence and/or absence of Fe^{2+} in $\text{M}_1\text{M}_2\text{M}_3$ sites, the number of bands varies from one in the tremolite up to three in actinolite (Jovanovski et al. 2009, also see Table 3). Considering the above discussion, the appearance of bands at 3643 and 3621 cm^{-1} in the spectra of K17-1 sample, which correspond to $\text{MgFe}^{2+}\text{Fe}^{2+}\text{-OH-}^{\text{A}}_{\square}$, $\text{Fe}^{2+}\text{Fe}^{2+}\text{Fe}^{2+}\text{-OH-}^{\text{A}}_{\square}$ configurations, respectively, supporting the result that amphibole type in the studied sample most likely belongs to the actinolite species (see Table 3). However, the absence of these bands in spectra of K17-2 sample can suggest that this sample has a similar chemical composition to the boundary of the tremolite, compared to those of K17-1 sample.

Table 4. Comparison between the chemical composition $X = ^{\text{C}}\text{Mg}/^{\text{C}}(\text{Mg} + \text{Fe}^{2+})$ derived from EMPA and from the Raman intensities of the OH-stretching modes (Leissner et al. 2015; Bersani et al. 2019) and from the position of the main Raman peak at low wavenumber 200-1200 cm^{-1} (Bersani et al. 2019).

sample	X_{EMPA}	Leissner et al. 2015 $X = \frac{3I_{\text{MgMgMg}} + 2I_{\text{FeMgMg}} + I_{\text{FeFeMg}}}{3I_{\text{MgMgMg}} + 3I_{\text{FeMgMg}} + 3I_{\text{FeFeMg}} + 3I_{\text{FeFeFe}}}$	Bersani et al. 2019 $X = (A_{12})/(1/3 + A_{12})$	Bersani et al. 2019 $X = 0.066*(v - 659.3)$
K17-1	0.83-0.85	0.82	0.86	0.77
K17-2	0.84-0.87	0.87	0.82	0.64
R050336	0.85	-	-	0.71

Bersani et al. (2019) obtained the relation between the position of the main band in the low wavenumber region (200-1200 cm^{-1}) and the chemical composition $X = \text{Mg}/(\text{Mg} + \text{Fe}^{2+})$ with standard error of 0.03 : $X = 0.066*(v - 659.3)$, where v is expressed in cm^{-1} and 659.3 is the v value for $X = 0$. We obtained $X = 0.77$ for K17-1 ($v = 671 \text{ cm}^{-1}$), which not very far from the value obtained by EMPA, and 0.64 for K17-2 ($v = 669 \text{ cm}^{-1}$) which is not in good agreement with EMPA data (Table 4). However, the use of this relation to estimate the Mg# (X value) from the Raman spectrum requires a very good wavenumber calibration of the spectrometer (Bersani et al. 2019).

In addition, Mg# (X value) is also calculated from the OH stretching bands' fractional intensities using the equation:

$$\frac{3I_{\text{MgMgMg}} + 2I_{\text{FeMgMg}} + I_{\text{FeFeMg}}}{3I_{\text{MgMgMg}} + 3I_{\text{FeMgMg}} + 3I_{\text{FeFeMg}} + 3I_{\text{FeFeFe}}} \quad (\text{Leissner et al. 2015}).$$

Results obtained based on this equation are comparable with those obtained by the equation proposed by Bersani et al. (2019) $X = (A_{12})/(1/3 + A_{12})$, where A_{12} is the ratio between the intensity of two bands, often the most intense ones. The latter equation can be used to obtain X composition even using noisy spectra, with just using the most intense bands emerging (Bersani et al. 2019). The X value calculated from both methods is in very good agreement with the EMPA data (Table 4). Although Raman bands may be sensitive to the

orientation of the crystal, however, it appears that the quantitative estimation of Mg# can be obtained from the fractional intensities of the OH-stretching bands by applying Raman spectroscopy to micrometer-sized actinolite grains in crude rough rock sample.

6. Conclusion

Secondary minerals formed after pseudomorph of primary minerals usually inherit shape of the original minerals, making it difficult to identify by ordinary petrography. Raman spectroscopy is a useful technique to perform non-destructive and quick analysis to characterize actinolite in rock samples. This study thus provides a new method to determine the Mg# of actinolite by applying Raman spectroscopy to micrometer-sized grains in crude rough.

References

- Alavi M (1994) Tectonics of the Zagros orogenic belt of Iran: new data and interpretations. *Tectonophysics* 229: 211–238.
- Anderson JL, Smith DR (1995) The effects of temperature and $f\text{O}_2$ on the Al-in-hornblende barometer. *American Mineralogist* 80: 549-559.

- Andò S, Garzanti E (2014) Raman spectroscopy in heavy-mineral studies. *Geological Society, London*, Special volume no. 386: 395-412.
- Andrut M, Gottschalk M, Melzer S, Najorka J (2000) Lattice vibrational modes in synthetic tremolite-Sr-tremolite and tremolite-richterite solid solutions. *Physics and Chemistry of Minerals* 27: 301-309.
- Apopei AI, Buzgar N (2010) The Raman study of amphiboles. *Analele Stiintifice de Universitatii AI Cuza din Iasi, Geologie* 56: 57-83.
- Apopei AI, Buzgar N, Buzatu A (2011) Raman and infrared spectroscopy of kaersutite and certain common amphiboles. *Analele Stiintifice de Universitatii AI Cuza din Iasi, Geologie* 57: 35-58.
- Apopei AI, Buzgar N, Damian G, Buzatu A (2014) The Raman study of weathering minerals from the Coranda-Hondol open pit (Certej gold-silver deposit) and their photochemical degradation products under laser irradiation. *The Canadian Mineralogist* 52: 1027-1038.
- Bard D, Yarwood J, Tylee B (1997) Asbestos fibre identification by Raman microspectroscopy. *Journal of Raman spectroscopy* 28: 803-809.
- Belluso E, Fornero E, Cairo S, Albertazzi G, Rinaudo C (2007) The application of micro-Raman spectroscopy to distinguish carlosturanite from serpentine-group minerals. *The Canadian Mineralogist* 45: 1495-1500.
- Bersani D, Aliatis I, Tribaudino M, Mantovani L, Benisek A, Carpenter MA, Gatta GD, Lottici PP (2018) Plagioclase composition by Raman spectroscopy. *Journal of Raman Spectroscopy* 49: 684-698.
- Bersani D, Andò S, Scrocco L, Gentile P, Salvioli-Mariani E, Fornasini L, Lottici PP (2019) Composition of Amphiboles in the Tremolite-Ferro-Actinolite Series by Raman Spectroscopy. *Minerals* 9: 491.
- Burns RG, Greaves C (1971) Correlations of infrared and Mossbauer site population measurements of actinolites. *American Mineralogist* 56: 2010-2033.
- Burns RG, Strens RG (1966) Infrared study of the hydroxyl bands in clinoamphiboles. *Science* 153: 890-892.
- Buzatu A, Buzgar N (2010) The Raman study of single-chain silicates. *Analele Stiintifice de Universitatii AI Cuza din Iasi, Geologie* 56: 107-126.
- Buzgar N, Apopei AI, Diaconu V, Buzatu A (2013) The composition and source of the raw material of two stone axes of Late Bronze Age from Neamt County (Romania)-A Raman study. *Analele Stiintifice de Universitatii AI Cuza din Iasi, Geologie* 59: 5-22.
- Castro A, Stephens WE (1992) Amphibole-rich polycrystalline clots in calc-alkaline granitic rocks and their enclaves. *The Canadian Mineralogist* 30: 1093-1112.
- Chen TH, Calligaro T, Pagès-Camagna S, Menu M (2004) Investigation of Chinese archaic jade by PIXE and μ Raman spectrometry. *Journal of Applied Physics A* 79: 177-180.
- Della Ventura G, Robert JL, Beny JM (1991) Tetrahedrally coordinated Ti^{4+} in synthetic Ti-rich potassic richterite: Evidence from XRD, FTIR, and Raman studies. *American Mineralogist* 76: 1134-1140.
- Della Ventura G, Robert JL, Beny JM, Raudsepp M, Hawthorne FC (1993) The OH-F substitution in Ti-rich potassium richterite: Rietveld structure refinement and FTIR and micro-Raman spectroscopic studies of synthetic amphiboles in the system $K_2O-Na_2O-CaO-MgO-SiO_2-TiO_2-H_2O-HF$. *American Mineralogist* 78: 980-987.
- Ernst WG, Wai CM (1970) Mössbauer, infrared, X-ray and optical study of cation ordering and dehydrogenation in natural and heat-treated sodic amphiboles. *American Mineralogist* 55: 1226-1258.
- Fornero E, Allegrina M, Rinaudo C, Mazziotti-Tagliani S, Gianfagna A (2008) Micro-Raman spectroscopy applied on oriented crystals of fluoro-edenite amphibole. *Periodico di Mineralogia* 77: 5-14.
- Ghalamghash J, Babakhani AR (1996) Geological Map of Kahak: *Geological Survey of Iran*, Scale 1:100000 Sheet.
- Gopal NO, Narasimhulu KV, Rao JL (2004) EPR, optical, infrared and Raman spectral studies of Actinolite mineral. *Spectrochimica Acta Part A: Molecular and Biomolecular Spectroscopy* 60: 2441-2448.
- Hawthorne FC, Oberti R (2007) Amphiboles: Crystal chemistry. In Hawthorne FC, Oberti R, Della Ventura G, Mottana A (2007) Amphiboles: Crystal Chemistry, Occurrence, and Health Issues. Reviews in Mineralogy and Geochemistry. *Mineralogical Society of America*.
- Hawthorne FC, Oberti R, Harlow GE, Maresch WV, Martin RF, Schumacher JC, Welch MD (2012) Nomenclature of the amphibole supergroup. *American Mineralogist* 97: 2031-2048.
- Huang E (2003) Raman Spectroscopic Study of Amphiboles. National Cheng Kung University (PhD thesis in Chinese).
- Huraiova M, Lengauer C, Abart R, Hurai V (2018) Compositional, structural and vibrational spectroscopic characteristics of feldspar megacrysts in alkali basalts from southern Slovakia. *Journal of Geosciences* 63: 215-226.
- Iezzi, G, Ventura GD, Bellatreccia F, Mastro SL, Bandli BR, Gunter ME (2007) Site occupancy in richterite-winchite from Libby, Montana, USA, by FTIR spectroscopy. *Mineralogical Magazine* 71: 93-104.
- Ivanov VG, Dyulgerov M, Oberti R (2019) Polarized Raman spectroscopy and lattice dynamics of potassic-magnesio-arfvedsonite. *Physics and Chemistry of Minerals* 46: 181-191.
- Jovanovski G, Makreski P, Kaitner B, Boev B (2009) Silicate minerals from Macedonia. Complementary use of vibrational spectroscopy and X-ray powder diffraction for identification and detection purposes. *Croatica Chemica Acta* 82: 363-386.
- Kaindl R, Többs DM, Haefeker U (2011) Quantum-mechanical calculations of the Raman spectra of Mg-

- and Fe-cordierite. *American Mineralogist* 96: 1568-1574.
- Kloprogge JT, Case MH, Frost RL (2001a) Raman microscopic study of the Li amphibole holmquistite, from the Martin Marietta Quarry, Bessemer City, NC, USA. *Mineralogical Magazine* 65: 775-785.
- Kloprogge JT, Visser D, Ruan H, Frost RL (2001b) Infrared and Raman spectroscopy of holmquistite, $\text{Li}_2(\text{Mg}, \text{Fe}^{2+})_3(\text{Al}, \text{Fe}^{3+})_2(\text{Si}, \text{Al})_8\text{O}_{22}(\text{OH})_2$. *Journal of materials science letters* 20: 1497-1499.
- Leake BE, Woolley AR, Birch WD, Burke EA, Ferraris G, Grice JD, Hawthorne FC, Kisch HJ, Krivovichev VG, Schumacher JC, Stephenson NC (2003) Nomenclature of amphiboles: additions and revisions to the International Mineralogical Association's 1997 recommendations. *The Canadian Mineralogist* 41: 1355-1362.
- Leake BE, Woolley AR, Birch WD, Burke EA, Ferraris G, Grice JD, Hawthorne FC, Kisch HJ, Krivovichev VG, Schumacher JC, Stephenson NC (2004) Nomenclature of amphiboles: additions and revisions to the International Mineralogical Association's amphibole nomenclature. *Mineralogical Magazine* 68: 209-215.
- Leissner L (2014) Crystal chemistry of amphiboles studied by Raman spectroscopy. Master thesis in Geoscience, University of Hamburg, Germany.
- Leissner L, Schlüter J, Horn I, Mihailova B (2015) Exploring the potential of Raman spectroscopy for crystallochemical analyses of complex hydrous silicates: I. Amphiboles. *American Mineralogist* 100: 2682-2694.
- Locock AJ (2014) An Excel spreadsheet to classify chemical analyses of amphiboles following the IMA 2012 recommendations. *Computers & Geosciences* 62: 1-11.
- Majumdar AS, Mathew G (2015) Raman-infrared (IR) spectroscopy study of natural cordierites from Kalahandi, Odisha. *Journal of the Geological Society of India* 86: 80-92.
- Makreski P, Jovanovski G (2009) Minerals from Macedonia: XXIII. Spectroscopic and structural characterization of schorl and beryl cyclosilicates. *Spectrochimica Acta Part A: Molecular and Biomolecular Spectroscopy* 73: 460-467.
- Makreski P, Jovanovski G, Dimitrovska S (2005b) Minerals from Macedonia: XIV. Identification of some sulfate minerals by vibrational (infrared and Raman) spectroscopy. *Vibrational Spectroscopy* 39: 229-239.
- Makreski P, Jovanovski G, Gajović A (2006) Minerals from Macedonia: XVII. Vibrational spectra of some common appearing amphiboles. *Vibrational Spectroscopy* 40: 98-109.
- Makreski P, Jovanovski G, Stojančeska S (2005a) Minerals from Macedonia XIII: Vibrational spectra of some commonly appearing nesosilicate minerals. *Journal of molecular structure* 744: 79-92.
- Mikouchi T, Miyamoto M (2000) Micro Raman spectroscopy of amphiboles and pyroxenes in the martian meteorites Zagami and Lewis Cliff 88516. *Meteoritics & Planetary Science* 35: 155-159.
- Otten MT (1984) The origin of brown hornblende in the Artfjället gabbro and dolerites. *Contributions to Mineralogy and Petrology* 86: 189-199.
- Petry R, Mastalerz R, Zahn S, Mayerhöfer TG, Völksch G, Viereck Götte L, Kreher Hartmann B, Holz L, Lankers M, Popp J (2006) Asbestos Mineral Analysis by UV Raman and Energy-Dispersive X-ray Spectroscopy. *Chemphyschem: a European journal of chemical physics and physical chemistry* 7: 414-420.
- Rinaudo C, Belluso E, Gastaldi D (2004) Assessment of the use of Raman spectroscopy for the determination of amphibole asbestos. *Mineralogical Magazine* 68: 455-465.
- Rinaudo C, Cairo S, Gastaldi D, Gianfagna A, Tagliani SM, Tosi G, Conti C (2006) Characterization of fluoroedenite by μ -Raman and μ -FTIR spectroscopy. *Mineralogical Magazine* 70: 291-298.
- Sbroscia M, Ventura GD, Iezzi G, Sodo A (2018) Quantifying the A-site occupancy in amphiboles: a Raman study in the OH-stretching region. *European Journal of Mineralogy* 30: 429-436.
- Shurvell HF, Rintoul L, Fredericks PM (2001) Infrared and Raman spectra of jade and jade minerals. *The Internet Journal of Vibrational Spectroscopy* 5, 4.
- Šontevska V, Jovanovski G, Makreski P, Raškovska A, Šoptrajanova B (2008) Minerals from Macedonia. XXI. Vibrational Spectroscopy as Identificational Tool for Some Phyllosilicate Minerals. *Acta Chimica Slovenica* 55: 757-766.
- Su W, Zhang M, Redfern SA, Gao J, Klemd R (2009). OH in zoned amphiboles of eclogite from the western Tianshan, NW-China. *International Journal of Earth Sciences* 98: 1299-1309.
- Susta U, Ventura GD, Hawthorne FC, Abdu YA, Day MC, Mihailova B, Oberti, R (2018) The crystal-chemistry of riebeckite, ideally $\text{Na}_2\text{Fe}_3^{2+}\text{Fe}_2^{3+}\text{Si}_8\text{O}_{22}(\text{OH})_2$: a multi-technique study. *Mineralogical Magazine* 82: 837-852.
- Waeselmann N, Schlüter J, Malcherek T, Della Ventura G, Oberti R, Mihailova B (2020) Nondestructive determination of the amphibole crystal-chemical formulae by Raman spectroscopy: One step closer. *Journal of Raman Spectroscopy*.
- Wang A, Dhamelincourt P, Turrell G (1988a) Infrared and low-temperature micro-Raman spectra of the OH stretching vibrations in cummingtonite. *Journal of Applied Spectroscopy* 42: 1451-1457.
- Wang A, Dhamelincourt P, Turrell G (1988b) Raman and infrared spectroscopic investigation of the cation distributions in amphiboles. *Journal of Molecular Structure* 175: 183-188.
- Wang A, Dhamelincourt P, Turrell G (1988c) Raman microspectroscopic study of the cation distribution in amphiboles. *Applied spectroscopy* 42: 1441-1450.

- Wang A, Jolliff BL, Haskin LA, Kuebler KE, Viskupic KM (2001) Characterization and comparison of structural and compositional features of planetary quadrilateral pyroxenes by Raman spectroscopy. *American Mineralogist* 86: 790-806.
- Whitney DL, Evans BW (2010) Abbreviations for names of rock-forming minerals. *American mineralogist* 95: 185-187.
- Wilkins RWT (1970) Iron-magnesium distribution in the tremolite-actinolite series. *American Mineralogist* 55: 1993-1998.
- Yang H, Konzett J, Prewitt CT, Fei Y (1999) Single-crystal structure refinement of synthetic M4K-substituted potassic richterite, $K(KCa)Mg_5Si_8O_{22}(OH)_2$. *American Mineralogist* 84: 681-684.
- Yazdi A, Ashja-Ardalan A, Emami MH, Dabiri R, Foudazi M (2019) Magmatic interactions as recorded in plagioclase phenocrysts of quaternary volcanics in SE Bam (SE Iran), *Iranian Journal of Earth Sciences* 11(3): 215-224.
- Yazdi A, ShahHoseini E, Razavi R (2016) AMS, A method for determining magma flow in Dykes (Case study: Andesite Dyke). *Research Journal of Applied Sciences* 11(3): 62-67.